

# A Dynamic Graph CNN with Cross-Representation Distillation for Event-Based Recognition

Yongjian Deng, *Member, IEEE*, Hao Chen, Bochen Xie, *Member, IEEE*,  
Hai Liu, *Senior Member, IEEE* and Youfu Li, *Fellow, IEEE*

**Abstract**—It is a popular solution to convert events into dense frame-based representations to use the well-pretrained CNNs in hand. Although with appealing performance, this line of work sacrifices the sparsity/temporal precision of events and usually necessitates heavy-weight models, thereby largely weakening the advantages and real-life application potential of event cameras. A more application-friendly way is to design deep graph models for learning sparse point-based representations from events. Yet, the efficacy of these graph models is far behind the frame-based counterpart with two key limitations: (i) simple graph construction strategies without carefully integrating the variant attributes (i.e., semantics, spatial and temporal coordinates) for each vertex, leading to biased graph representation; (ii) deficient learning because the lack of well pretraining models available. Here we solve the first problem by introducing a new event-based graph CNN (EDGCN), with a dynamic aggregation module to integrate all attributes of vertices adaptively. To alleviate the learning difficulty, we propose to leverage the dense representation counterpart of events as a cross-representation auxiliary to supply additional supervision and prior knowledge for the event graph. To this end, we form a frame-to-graph transfer learning framework with a customized hybrid distillation loss to well respect the varying cross-representation gaps across layers. Extensive experiments on multiple vision tasks validate the effectiveness and high generalization ability of our proposed model and distillation strategy<sup>1</sup>.

## I. INTRODUCTION

**E**ACH pixel of event cameras is independent and can report an event when detecting logarithmic brightness changes. This particular working principle endows event cameras with high dynamic range, low power consumption, and high temporal resolution with data non-redundancy, thus holding huge potentials on mobile and wearable devices<sup>2</sup>.

Yongjian Deng is with the College of Computer Science, Beijing University of Technology, Beijing 100124, China. yjdeng@bjut.edu.cn.

Bochen Xie and Youfu Li are with Department of Mechanical Engineering, City University of Hong Kong, Kowloon, Hong Kong SAR. {boxie4-c@my., meyfli}@cityu.edu.hk.

Hao Chen is with School of Computer Science and Engineering, Southeast University, and Key Lab of Computer Network and Information Integration (Southeast University), Ministry of Education, Nanjing 211189, China. haochen593@gmail.com.

Hai Liu is with the National Engineering Research Center for E-Learning, Central China Normal University, Wuhan 430079, China hailiu0204@ccnu.edu.cn.

© 20XX IEEE. Personal use of this material is permitted. Permission from IEEE must be obtained for all other uses, in any current or future media, including reprinting/republishing this material for advertising or promotional purposes, creating new collective works, for resale or redistribution to servers or lists, or reuse of any copyrighted component of this work in other works.

<sup>1</sup>Core components of our codes are submitted with supplementary material and will be made publicly available upon acceptance.

<sup>2</sup>A survey about event-based applications can be found in [1]

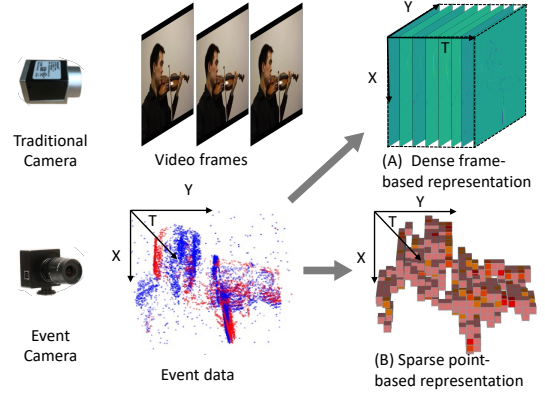


Fig. 1. Visual comparison between outputs from traditional cameras and event cameras. (a) Frame-based representations obtained by integrating events along the time axis. (b) The point-based representation (depicted in Eq. III-A) we adopted can better exploit the sparsity of event data than its frame-based counterpart. X, Y and T represent spatial and temporal dimensions of event data. The colors of events stand for different polarities.

However, how to represent and learn from this special data format (Eq. 1) effectively is still inconclusive.

Current works on representing event data mainly lie in two lines: (1) **Frame-based methods** [2]–[7] that sacrifice the real-life application potentials (including the data sparsity and motion precision) to make event data compatible with pre-trained CNNs by integrating sparse event signals into dense frame-based representations; (2) **Point-based methods** that take the sparse representation (e.g., a single event or a set of regional events) as an input unit to protect the sparsity and temporal structure of event streams, including directly regard event streams as 3D point clouds and adopt PointNet-like architectures [8]–[10] or build event-based graphs [11]–[16] to aggregate local features and encode 2D continuous semantics. With discrepancies among different event attributes (e.g., spatial, temporal coordinates, and features) and limited labeled data, existing point-based methods are suffering from either biased graph representation or inadequate training.

In this work, we follow the point-based solution to fully respect the inherent advantages of event cameras and solve the following key problems in this community:

(1) *How to define neighborhood space for vertices of an event-based graph by considering all attributes of each vertex simultaneously and differentially.*

(2) *How to facilitate the learning of event graphs by fully exploring the potential of events without resorting to extra*

data.

We address the first issue by designing a novel dynamic voxel-wise graph CNN (EDGCN). Compared to frame-based and other point-based solutions, such a representation strategy [14], [15] can hold noticeable advantages in encoding 2D coherent semantics while keeping motion accuracy. As a voxel holds heterogeneous attributes, i.e., spatial/temporal coordinates and semantic features encoded by corresponding events, how to involve these attributes comprehensively, model their dependencies and assign their well-matched contributions in measuring the cross-vertex edges is the key problem to construct a graph. Previous approaches build graphs by either merely taking spatio-temporal distances into account [12], [15], [16] or scaling these attributes equally [11], [13], [14], failing to consider their great discrepancies. To remove these biases, we involve all attributes to determine the dependencies across vertices and respect cross-attribute gaps by dynamically learning and activating the contribution of each attribute. Specifically, we devise an event-based dynamic aggregation layer (EDAL), consisting of a multi-attribute joint learning branch to learn the integration policy for defining the neighborhood, and another rebalance design to avoid the shrinking of spatial-temporal coordinates in the attribute aggregation process as their dimensions are much smaller than the one of semantic features.

To remove the bottleneck towards well learning an event-based graph model, we take full use of the original event streams and map them to an additional frame-based representation branch, and borrow the valuable prior knowledge in well-trained CNNs to facilitate the training of the event graph via a frame-to-graph distillation framework. Notably, a hybrid distillation loss, composed of an intermediate feature-level contrastive loss [17] and inference-level distillation loss [18], [19], is customized to consider the varying frame-graph discrepancies across shallow and deep layers and enable the transfer of multi-scale semantics. Compared to previous frame-to-frame transfer learning methods proposed in the frame-based line [20]–[23], our source and target inputs are all from the same event data without using additional paired image data, thus holding better generalization ability. Also, our frame-to-graph transfer problem is more difficult due to the large discrepancy between the two different representation formats.

By solving the above two problems, our event graph holds adaptive learning ability in edge definition and feature aggregation, a more decent training scheme, and strong generalization ability with widely better accuracy while much fewer parameters and faster inference time. The main contributions of this paper are summarized as follows:

- (1) We introduce a novel graph CNN for event data, where the cross-vertex dependency is determined by the joint representation from all attributes of vertices in a learnable manner.
- (2) It is the first cross-representation distillation (frame-to-graph distillation). we carefully analyze the variant discrepancy between frame and graph representation in different layers and use corresponding constraints to distill different layers. This discrepancy is a new problem not studied in

previous distillation works

(3) By solving the event-graph construction and training bottlenecks, our model shows noticeable accuracy gains with extremely low model and computation complexity.

(4) Extensive experiments validate the efficacy of our proposed event graph and learning strategy on various downstream tasks, verifying the high generalization ability of our model.

## II. RELATED WORK

**Event-based learning** Current event-based studies focus on designing deep models for event-based processing. These deep models can be categorized as frame-based and point-based methods. Frame-based methods commonly integrate events into dense representations and adapt these representations to CNNs for further processing. Benefiting from prior knowledge contained in pretrained CNNs, these approaches achieve the highest performance on multiple vision tasks, *e.g.*, event-based recognition [2]–[6], video reconstruction [7], [24], [25], optical flow estimation [26]–[28]. Nevertheless, they usually sacrifice the sparsity of event data, leading to redundant computation and high model complexity [13], [29], thereby limiting event-based applications on mobile devices, edge computing, *etc.*

For the above reasons, point-based methods gradually become more popular, where the sparsity of events is exploited to design recognition models with low model complexity and fast inference speed. Spiking neural networks (SNNs) [30], [31] are first applied to event data because of their sparse and asynchronous natures. However, training classic SNNs is intractable due to the lack of mature optimizing methods. Though methods in [32], [33] mitigate this issue by combining them with CNNs, the introduced additional computations weaken the superiority of SNNs. Inspired by the 3D vision, [9], [10] build PointNet-like architectures for event data. However, these structures hold limited capability in aggregating local features adaptively. Graph-based approaches [11]–[13], [16], [29] are then proposed to address this problem through raising heuristic neighborhood definition *w.r.t* properties of events to better aggregate vertices. To endow each vertex in the graph with local semantics, [14], [15] further present a novel voxel-wise representation for each vertex. Such a voxel-wise graph construction strategy [15] has achieved top performance on multiple tasks among the point-based community. Compared to the frame-based counterpart, graph-based methods are much more lightweight and show better prospects on various downstream tasks and real-life application scenarios. Even this, the critical stage that determining each vertex’s neighborhood is typically performed by either merely considering spatio-temporal distances or scaling these attributes (i.e., features, spatial and temporal coordinates) equally without considering the attributes comprehensively and distinguishably, leading to biased feature aggregation and graph topology. Instead, we embed features of vertices from their neighbors by dynamically learning a joint representation from all vertices’ attributes.

**Transfer learning on event data** Many transfer learning studies have been proposed to mitigate the difficulties in

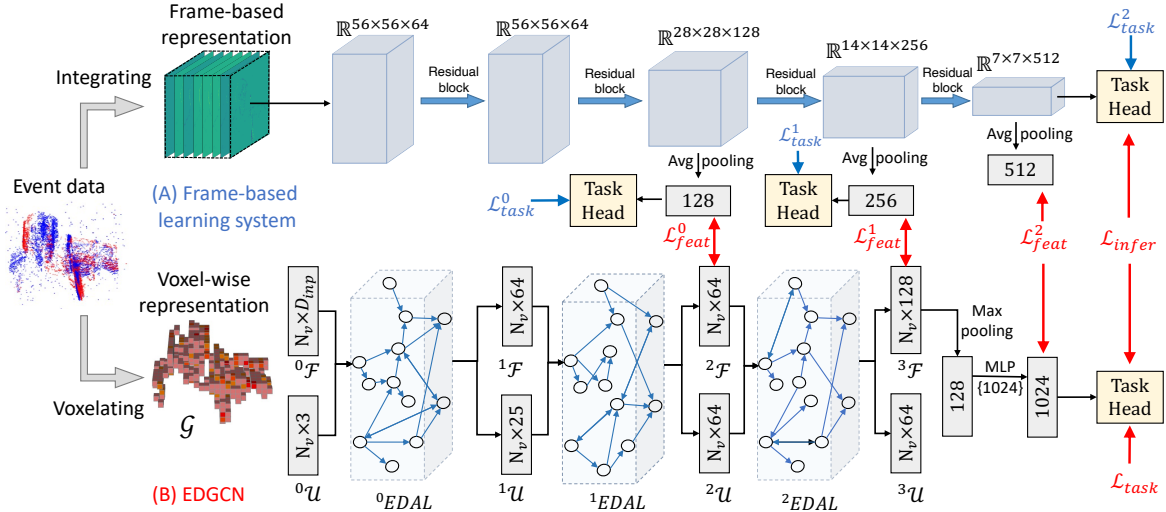


Fig. 2. The pipeline of our proposed method. Two different representations derived from the same input are taken as input for the frame-based model (A) and the point-based model, *i.e.*, EDGCN (B). The resent-like structure is chosen as an example to represent the frame-based model. “MLP” stands for multi-layer perceptron, numbers in bracket are layer sizes. The function of graph learning module EDAL and losses are depicted in Eq. III-C and Eq. III-D, respectively. Losses with blue color are used for frame-based model training, and red color are imposed when optimizing the EDGCN with CRD.

training event-based models. For instance, [34]–[36] achieve knowledge transferring by converting event data to RGB images for exploiting the knowledge contained in pretrained CNNs. However, the conversion process largely introduces additional computation cost and limits real-life practicability. [20]–[23], [37], [38] adopt similar 2D-2D transfer schemes by introducing extra supervision to facilitate the learning of event branch from additional visual modalities which are not always available in practice. Some other works [39]–[41] try to supplement event-based datasets by simulating event data from traditional videos. However, artifacts are inevitably imposed during the simulation. Instead, our proposed cross-representation distillation scheme explores the transferable knowledge inside the original source data by additionally forming the given event streams to an auxiliary frame-based representation branch without resorting to any additional data sources and thus holding a wider range of applications. The learning of the event graph branch is then advanced by a frame-to-graph distillation loss.

### III. APPROACH

In this work, we devise a novel event-based dynamic graph CNN (EDGCN) and a cross-representation distillation strategy (CRD) to boost its learning sufficiency further. The pipeline of our proposed method is illustrated in Eq. 2, which contains the following key steps: (1) Voxelizing the original events as the vertex of the graph model. (2) Using successive event-based dynamic aggregation layers (EDAL) to aggregate contexts gradually. (3) Paralleled to the event graph branch, we map the original events to a frame-based branch as the teacher to promote the learning of the EDGCN branch via the customized cross-representation distillation loss. (4) The EDGCN is then appended with different inference heads for various tasks. The following sections will clarify detailed designs and implementations in these steps.

#### A. Event-based representation

**Event data** Each event  $e_i$  holds three properties: the occurred location  $((x_i, y_i))$ , the triggered timestamp  $(t_i)$ , and the polarity  $(p_i \in \{-1, 1\})$ . Particularly, the positive  $p$  denotes the brightness increase and vice versa.

**Voxel-wise representation** The output of event cameras is noisy and unevenly distributed in  $x$ - $y$ - $t$ - $p$  space. Thus, taking original events as vertices as done in previous point-based models may hold limited robustness and generalization ability and the indispensable heavy sub-sampling processing leads to inevitably severe information loss. Instead, voxel-wise representations [14], [15] are adopted here retain more local semantics and motion cues while being robust to noise events and maintaining the sparsity advantage. In specific, event streams  $(\{e_i\}_N = \{x_i, y_i, t_i, p_i\}_N)$  is firstly partitioned into voxels with the voxel size  $(v_x, v_y, v_t)$ . Then,  $N_v$  voxels containing the largest number of events are reserved as vertices  $(\mathcal{V})$  of the event-based graph  $(\mathcal{G})$ . Here, we denote the left-upper location of a vertex  $(\mathcal{V}_i)$  as its coordinate attribute  $({}^0\mathcal{U}_i = (x_i^v, y_i^v, t_i^v))$ . Finally, the feature  $({}^0\mathcal{F}_i \in \mathbb{R}^{D_{inp}})$  of the  $i$ -th vertex  $(\mathcal{V}_i)$  is obtained through event-wise integration formulated by the function  $\Omega$ , where  $D_{inp} = v_x v_y$ .

#### B. EDGCN

As three attributes describe each vertex with different physical meanings: spatial position, triggered time, and local semantics, we believe that how to involve these attributes comprehensively, model their dependencies and assign their well-matched contributions in measuring the cross-vertex edges is the key issue to construct an event-based graph. We answer this question with dynamic aggregation layers to explicitly highlight the dynamics in the graph learning process, including neighborhood determination, feature aggregation, and attribute update. The dynamically updated graph allows our model to improve its neighborhood definition accuracy and feature

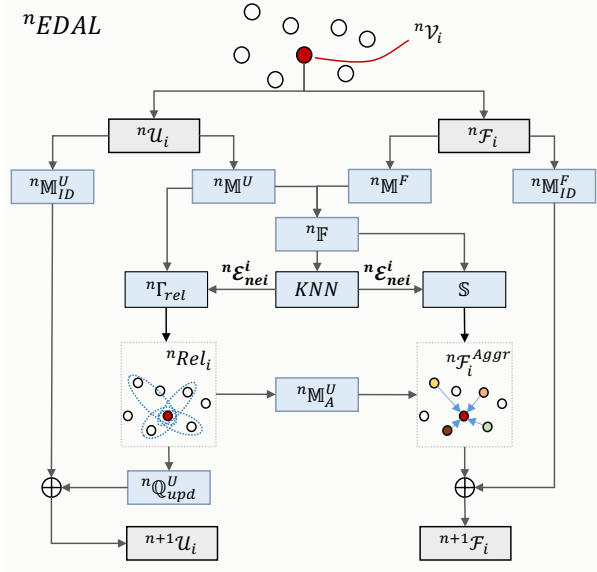


Fig. 3. An illustration of how the  $n$ -th EDAL aggregates features for vertex  ${}^n\mathcal{V}_i$  from its neighbors. The function of each notation shown in the figure is detailed in Eq. III-C.  $\oplus$ : element-wise addition.

aggregation efficacy by continuously refining vertex attributes at each layer.

### C. Dynamic aggregation layer (EDAL)

The main component of our EDGCN, namely EDAL, is schematized in Eq. 3. Its workflow is detailed successively as follows.

**Neighborhood definition** We suppose that the  $i$ -th vertex  ${}^n\mathcal{V}_i$  is an input vertex to  $n$ -th EDAL with coordinate and feature attributes  $Attr({}^n\mathcal{V}_i) : ({}^n\mathcal{U}_i \in \mathbb{R}^{in D_u}, {}^n\mathcal{F}_i \in \mathbb{R}^{in D_f})$ . The goal of EDAL is to define neighborhood space for each vertex by considering all its attributes and aggregating attributes from its neighbors attentively. Considering the large discrepancy in spatial position, triggered time, and features of local semantics, we argue that projecting the  $Attr({}^n\mathcal{V}_i)$  to a unified feature space with Eq. 1 is in demand.

$${}^n\mathcal{P}_i^F = {}^n\mathbb{M}^F({}^n\mathcal{F}_i), \quad {}^n\mathcal{P}_i^U = {}^n\mathbb{M}^U({}^n\mathcal{U}_i), \quad (1)$$

where  ${}^n\mathbb{M}^F$  and  ${}^n\mathbb{M}^U$  are *MLPs* for feature projection. The obtained representations  ${}^n\mathcal{P}_i^F$  and  ${}^n\mathcal{P}_i^U \in \mathbb{R}^{in D_f}$  in the same feature space can then be fused as a joint representation  ${}^n\mathcal{P}_i^{fuse}$  for vertex  ${}^n\mathcal{V}_i$ . Notably, we achieve the  ${}^n\mathcal{P}_i^{fuse} \in \mathbb{R}^{out D_f}$  through a fusion module ( ${}^n\mathbb{F}$ ) consisting of an addition operation followed by a *MLP*. Next, we adopt the K-Nearest neighbor algorithm (*KNN*) on this joint representation to find the most relevant  $N_n$  neighbors of  ${}^n\mathcal{V}_i$  in the  $\mathcal{G}$ . Here, we denote the set of edges between vertex  ${}^n\mathcal{V}_i$  and its neighbors as  ${}^n\mathcal{E}_i^{nei} \in \mathbb{R}^{N_n}$ .

A straightforward approach to aggregate features for  ${}^n\mathcal{V}_i$  is applying pooling operations to its neighbors [42]. However, such a way that equally regards all attributes without distinguishing and explicitly rebalancing their contributions will gradually weaken the importance of coordinates with the

layer-by-layer aggregation going, while in theory the coordinates, containing irreplaceable spatial and motion cues, should always be highlighted in the aggregation stream to protect the original event structure. We avoid this difficulty from two views. (1) **Attentive feature aggregation.** We introduce coordinate distance to reweigh feature attributes of vertices' neighbors (Eq. 2) to prevent the vanishing of spatio-temporal clues contained in coordinate attributes. (2) **Coordinate attribute update.** We update the coordinate attributes with present spatio-temporal distances among the vertex's neighbors to embed motions explicitly. Detailed implementations are described in the following two segments.

**Attentive feature aggregation** We calculate attention scores *w.r.t* the coordinate attribute for neighbors of  ${}^n\mathcal{V}_i$  as formulated in Eq. 2.

$${}^nRel_i = \sum_{j:(i,j) \in {}^n\mathcal{E}_i^{nei}} {}^n\Gamma_{rel}({}^n\mathcal{P}_i^U, {}^n\mathcal{P}_i^U - {}^n\mathcal{P}_j^U) \quad (2)$$

$${}^nScore_i = {}^n\mathbb{M}_A^U({}^nRel_i),$$

where the function  ${}^n\Gamma_{rel}$  is used for concatenating its two inputs and stacking them under the constraint  $(j : (i, j) \in {}^n\mathcal{E}_i^{nei})$ .  ${}^nRel_i \in \mathbb{R}^{2^{in} D_f}$  represents the locally spatio-temporal relations derived from projected coordinate attributes  ${}^n\mathcal{P}^U$  of  ${}^n\mathcal{V}_i$  and its neighbors. Then, the function  ${}^n\mathbb{M}_A^U$ , a *MLP* with the Softmax activation, is imposed for mapping the input in  $\mathbb{R}^{N_n \times 2^{in} D_f}$  to a vector of attentive scores  ${}^nScore_i \in \mathbb{R}^{N_n}$ . Next, we can aggregate features for vertex attentively as described in Eq. 3.

$${}^n\mathcal{F}_i^{Aggr} = \sum {}^nScore_i * (\mathbb{S}_{j:(i,j) \in {}^n\mathcal{E}_i^{nei}} ({}^n\mathcal{P}_j^{fuse})), \quad (3)$$

where  $\mathbb{S}$  works for stacking joint representations ( ${}^n\mathcal{P}_j^{fuse} \in \mathbb{R}^{out D_f}$ ) of all vertex's neighbors and its output is in  $\mathbb{R}^{N_n \times out D_f}$ . The attentive scores  ${}^nScore_i$  can then be applied to re-weight and obtain the aggregated features  ${}^n\mathcal{F}_i^{Aggr} \in \mathbb{R}^{out D_f}$  for vertex  ${}^n\mathcal{V}_i$  through a summation operation over its neighbors.

**Coordinate attribute update** We depict the derivation of updating coordinate attributes by  ${}^n\mathcal{U}_i^{upd} = {}^n\mathbb{Q}_{upd}^U({}^nRel_i)$ , where  ${}^nRel_i$  is obtained in Eq. 2,  ${}^n\mathbb{Q}_{upd}^U$  consists of an average pooling followed by a *MLP* for feature aggregation and feature projection. After these two processes, the updated coordinate attribute  ${}^n\mathcal{U}_i^{upd} \in \mathbb{R}^{in D_f}$  of  ${}^n\mathcal{V}_i$  can be achieved. By updating the coordinate attribute of each vertex with local spatio-temporal relations with its neighbors, the vertex is equipped with spatio-temporal positions and local motion associations simultaneously, which will be transmitted to the neighbor definition and feature aggregation processes in the following layer.

**Shortcut connection** In the EDAL, two shortcut connections are included for both coordinate and feature attributes of vertices in the graph. As formulated in Eq. 4, two *MLPs* ( ${}^nM_{ID}^U$  and  ${}^nM_{ID}^F$ ) are applied to input attributes  ${}^n\mathcal{U}_i$  and  ${}^n\mathcal{F}_i$  respectively. Finally, we add the attained features from  ${}^nM_{ID}^U$  and  ${}^nM_{ID}^F$  to our achieved updated coordinate attribute ( ${}^n\mathcal{U}_i^{upd}$ ) and aggregated features ( ${}^n\mathcal{F}_i^{Aggr}$ ) to obtain the final

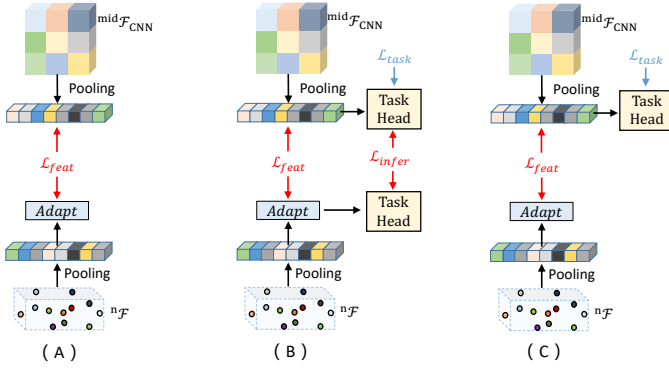


Fig. 4. Different choices of knowledge transferring between intermediate features from frame-based models ( $mid_{\mathcal{F}_{CNN}}$ ) and the proposed EDGCN ( ${}^n\mathcal{F}$ ). The *Adapt* module is a *MLP* for dimension alignment between two feature vectors. Losses with blue color are used for frame-based model training, and red color are imposed when transfer learning is performed. We adopt (C) as our choice and detail the reason in Eq. IV-E.

output of  $n$ -th EDAL, *i.e.*,  ${}^{n+1}\mathcal{U}_i \in \mathbb{R}^{in D_f}$  and  ${}^{n+1}\mathcal{F}_i \in \mathbb{R}^{out D_f}$ .

$$\begin{aligned} {}^{n+1}\mathcal{U}_i &= {}^n\mathcal{U}_i^{upd} + {}^nM_{ID}^U({}^n\mathcal{U}_i), \\ {}^{n+1}\mathcal{F}_i &= {}^n\mathcal{F}_i^{Aggr} + {}^nM_{ID}^F({}^n\mathcal{F}_i), \end{aligned} \quad (4)$$

**Network structure** The structure of the EDGCN is the same for all datasets except for the sub-stream task head. Specifically, three EDALs are cascaded to extract discriminative features from event data sequentially. For recognition tasks, *e.g.*, object recognition and action recognition, we apply a Max pooling operation followed by a *MLP* after the third EDAL and then feed the output of this *MLP* to a fully connected layer for categorical prediction. As for the detection task, we follow the setting provided by [13] to apply a YOLO-based detection head [43] to our extracted event-based contexts for object detection.

#### D. Cross-representation distillation (CRD)

As shown in Eq. 2, in our cross-representation distillation framework, the teacher network is a frame-based learning branch crafted by integrating original event data to frames and learning them starting from well-trained CNNs, while the student network is our *EDGCN* model. Then, a combined distillation constraint working on different layers is tailored to fulfill this transfer.

**Distillation losses** The key issue to fulfill this difficult frame-to-graph transfer is the design of the distillation loss to carefully regard the varying cross-representation discrepancy in different layers. To this end, we design a hybrid distillation containing two views: (1) Inference-level that distill contexts from the final predicting outputs. For instance, we apply the distillation loss proposed in [18] for classification tasks and the L1 loss [19] for regression-based tasks like position estimating in object detection. (2) Feature-level constraints that transfer hints from intermediate features of frame-based models. The knowledge transfer of intermediate features has been verified to effectively improve the training effect of the model to be transferred. However, for traditional CNNs and

TABLE I  
STATISTICS OF DIFFERENT DATASETS AND PARAMETER SETTINGS FOR REPRESENTATION CONSTRUCTION.

| Datasets     | N-Cal [46] | CIF10 [47] | N-C [31] | DVS128 [48] |
|--------------|------------|------------|----------|-------------|
| Duration     | 300 ms     | 1280 ms    | 100 ms   | 6000 ms     |
| Classes      | 101        | 10         | 2        | 11          |
| Samples      | 8246       | 10000      | 24029    | 1342        |
| $(v_x, v_y)$ | (10, 10)   | (10, 10)   | (5, 5)   | (5, 5)      |
| $v_t$        | 25 ms      | 60 ms      | 25 ms    | 40 ms       |
| $N_v$        | 2048       | 2048       | 512      | 1024        |

our EDGCN, their learning logic for event data from shallow to deep might be totally different. Thus, hard constraints (*e.g.*, L1/L2 distance) [44] would be too strict for our transfer task. For this reason, we exploit the contrastive loss, NT-Xent [17], [45], to realize the transfer by enlarging the correlation of intermediate features from two networks. In specific, three variants to equip NT-Xent loss in the CRD are proposed in Eq. 4, where the method in Eq. 4.(C) is adopted as the final choice. In Eq. IV-E, we detail the reason for our choice and its advantages in conjunction with experimental results.

**Optimization** The whole training process of our study can be divided into two parts. First, the training process of frame-based models with task-specific loss solely is described by  $\mathcal{L}_{total}^{frame} = \sum_i^{N_t} \mathcal{L}_{task}^i$ , where  $\mathcal{L}_{task}^i$  are task-specific losses. They are applied to multiple prediction layers individually (Eq. 2).  $N_t$  represents the number of intermediate features used for cross-representation learning. Next, we optimize our proposed EDGCN with the loss for task-specific supervision ( $\mathcal{L}_{task}$ ), the loss for inference-level knowledge transferring ( $\mathcal{L}_{infer}$ ) and a series of contrastive losses ( $\mathcal{L}_{feat}^i$ ) for feature-level distillation as described in Eq. 5.

$$\mathcal{L}_{total}^{EDGCN} = \lambda \mathcal{L}_{task} + (1 - \lambda) \mathcal{L}_{infer} + \sum_i^{N_t} \mathcal{L}_{feat}^i, \quad (5)$$

where  $\lambda$  control the contribution of the first two components in the training process and set it as 0.5 for all experiments.

## IV. EXPERIMENTAL RESULTS

We evaluate our proposed method on several tasks, *e.g.*, object classification, action recognition and object detection. Besides, we validate the superiority of the EDGCN on the model complexity (measured in the number of trainable parameters) and the number of floating-point operations (FLOPs). Then, the efficacy of the proposed CRD and its generalizability on multiple vision tasks is validated.

**Implementation details** We choose ResNet [49] as the backbone of frame-based models used for applying CRD to object classification and object detection tasks and adopt I3D-R (w/ ResNet50) [50] for the action recognition task, where ResNet is pretrained on ImageNet and I3D-R is pretrained using Kinetics-400 dataset. We train them using the Adam optimizer with batch size 32 and an initial learning rate ( $lr$ )

TABLE II  
COMPARISON OF MODELS *w.r.t* CLASSIFICATION ACCURACY.

| Method                         | Type <sup>§</sup> | N-Cal        | N-C          | CIF10        |
|--------------------------------|-------------------|--------------|--------------|--------------|
| Pretrained on ImageNet [51]    |                   |              |              |              |
| EST [2]                        | F                 | 0.837        | 0.925        | 0.749        |
| M-LSTM [3]                     | F                 | 0.857        | 0.957        | 0.730        |
| MVF-Net [5]                    | F                 | <b>0.871</b> | <b>0.968</b> | <b>0.762</b> |
| Without pretraining            |                   |              |              |              |
| EST [2]                        | F                 | 0.753        | 0.919        | 0.634        |
| M-LSTM [3]                     | F                 | 0.738        | 0.927        | 0.631        |
| MVF-Net [5]                    | F                 | 0.687        | 0.927        | 0.599        |
| AsyNet [4]                     | F                 | 0.745        | 0.944        | 0.663        |
| EventNet [10]                  | P                 | 0.425        | 0.750        | 0.171        |
| RG-CNNs [11]                   | P                 | 0.657        | 0.914        | 0.540        |
| EvS-S [12]                     | P                 | 0.761        | 0.931        | 0.680        |
| EV-VGCNN [14]                  | P                 | 0.748        | 0.953        | 0.670        |
| AEGNN [13]                     | P                 | 0.668        | 0.945        | -            |
| VMV-GCN [15]                   | P                 | 0.778        | 0.932        | 0.690        |
| EV-Transformer [16]            | P                 | 0.789        | 0.954        | 0.709        |
| <b>Ours</b> <sup>†</sup>       | P                 | <b>0.801</b> | <b>0.958</b> | <b>0.716</b> |
| <b>Ours + CRD</b> <sup>‡</sup> | P                 | <b>0.835</b> | <b>0.963</b> | <b>0.752</b> |

†: Performance of the model trained solely. ‡: Performance of the model trained with CRD. § : F:frame-based method; P:point-based method.

of  $1e-4$ , which is reduced by a factor of 2 after 20 epochs. The dense input of these frame-based models is VoxelGrid [26]. For the EDGCN, we keep its network structure (Eq. 2) unchanged for all datasets except for its task head. We use SGD optimizer with an initial  $lr$  of  $1e-1$  for object classification and action recognition, and reduce the  $lr$  until  $1e-4$  using cosine annealing. We choose Adam optimizer with batch size 32 for detection, and reduce  $lr$  starting from  $1e-2$  by a factor of 2 after 20 epochs. The settings are consistent for training the EDGCN solely and with CRD. We list the statistics of adopted datasets and their settings of voxel-wise representation construction.

#### A. Object classification

Event-based object classification is an essential application since event cameras can recognize objects more accurately than traditional cameras in scenarios with severe motion blur and extreme lighting conditions. In this work, we select three challenging datasets commonly used for evaluating event-based object classification, *i.e.*, N-Cal [46], N-C [47], and CIF10 [47] (Eq. I). The ResNet-18 is the backbone of the frame-based model that we employed for optimizing EDGCN with CRD, and its performance on N-Cal, N-C, and CIF10 is 0.868, 0.964, and 0.757. The cross-entropy loss is utilized as  $\mathcal{L}_{task}$  for the model’s training.

**Classification accuracy** We compare the proposed method with SOTA methods falling in both point-based and frame-based categories. The Eq. II presents that methods with graph-based learning (RG-CNNs, EvS-S, EV-VGCNN, AEGNN, VMV-GCN, EV-Transformer and ours) are prevalent *w.r.t*

TABLE III  
COMPARISON OF MODELS *w.r.t* THE ELEVEN-POINT MEAN AVERAGE PRECISION (mAP) ON THE EVENT-BASED OBJECT DETECTION TASK.

| Methods         | Type | N-Cal (mAP $\uparrow$ ) |
|-----------------|------|-------------------------|
| YOLE [52]       | F    | 0.398                   |
| Asynet [4]      | F    | 0.643                   |
| NvS-S [12]      | P    | 0.346                   |
| AEGNN [13]      | P    | 0.595                   |
| <b>Ours</b>     | P    | <b>0.657</b>            |
| <b>Ours+CRD</b> | P    | <b>0.711</b>            |

classification accuracy over other point-based methods. Notably, the proposed EDGCN achieves top performance among these graph-based approaches, revealing the effectiveness of our proposed learning model. We attribute these improvements to the EDAL that can aggregate features for vertices considering all attributes dynamically, which allows us to efficiently and precisely extract the semantics of events. Excitedly, the introduced CRD can improve the performance of the EDGCN by a large margin. It proves that our CRD can successfully utilize the pretrained weights of CNNs to ease the learning of our graph model and improve its representation ability, even with large image-to-graphs gaps. However, our model, largely improved by the CRD scheme, still lags behind some frame-based methods (e.g., the MVF-Net) that are with pretraining. We attribute this to the much smaller discrepancy between image-frame than our frame-graph, allowing those frame-based methods to directly use the model weights well well-trained with large-scale datasets.

Moreover, Eq. IV shows that our method holds large advantages in model complexity and computational cost over other approaches.

#### B. Action recognition

*Will be released soon*

#### C. Object detection

Event-based object detection is an emerging topic to simultaneously solve object localization and categorization. This task requires event-based models with powerful semantics and motion encoding capabilities. We conduct experimental comparisons for this task on the N-Cal dataset, which is a single object detection dataset containing 101 classes. The ResNet-34 is used as the backbone of the frame-based teacher branch for our CRD, and its performance on N-Cal is 0.76. Following the setup in [13], we use a collection of losses (a weighted sum of class, bounding box offset and shape as well as prediction confidence losses) as the  $\mathcal{L}_{task}$  for training.

**Detection performance** We utilize the eleven-point mean average precision (mAP) to measure our models on the detection task. From results in Eq. III and Eq. IV, we conclude that our approach achieves large improvement on mAP over others with much fewer parameters and computational costs. More importantly, the proposed EDGCN trained solely exceeds other

TABLE IV  
COMPARISON OF MODELS ON THE MODEL COMPLEXITY (#PARAMS) AND THE NUMBER OF FLOPS.

| Method         | Type | #Params       | GFLOPs      | Time      |
|----------------|------|---------------|-------------|-----------|
| EST [2]        | F    | 21.38 M       | 4.28        | 6.41 ms   |
| M-LSTM [3]     | F    | 21.43 M       | 4.82        | 10.89 ms  |
| MVF-Net [5]    | F    | 33.62 M       | 5.62        | 10.09 ms  |
| AsyNet [4]     | F    | 3.69 M        | 0.88        | -         |
| EventNet [10]  | P    | 2.81 M        | 0.91        | 3.35 ms   |
| PointNet++ [9] | P    | 1.76 M        | 4.03        | 103.85 ms |
| RG-CNNs [11]   | P    | 19.46 M       | 0.79        | -         |
| EV-VGCNN [14]  | P    | 0.84 M        | 0.70        | 7.12 ms   |
| AEGNN [13]     | P    | 20.4 M        | 0.75        | -         |
| VMV-GCN [15]   | P    | 0.86 M        | 1.30        | 6.27 ms   |
| <b>Ours</b>    | P    | <b>0.77 M</b> | <b>0.57</b> | 3.84 ms   |

graph-based models such as NvS-S and AEGNN by a large margin, indicating the superiority of our EDGCN. Besides, CRD also largely boosts the detection performance in addition to object and action recognition tasks, suggesting the well generalizability of our proposed learning scheme.

#### D. Complexity analysis

We follow the calculation approach in [11], [14] to compute the complexity and FLOPs of models designed for object classification on the N-Cal. The listed results in Eq. IV show that our approach can perform classification tasks with extremely low model complexity and computational cost, indicating the high efficiency the learning system holds in extracting representative features from event data. We further measure the models’ inference time on the N-C dataset to show the practical potential of our model. The proposed method is implemented with PyTorch on an Nvidia RTX 3090. As shown in Eq. IV, our approach can realize leading performance on the N-C with only 3.84 ms processing time (equivalent to a frame-rate of 260 Hz) for each sample, suggesting its practical value in high-speed scenarios. Although our approach is slightly slower than EventNet, the much higher performance of our method (see Eq. IV) demonstrates its better efficacy and generalization ability.

#### E. Ablation study

In this section, we evaluate our method through various settings, where setup series I is for evaluating core modules of EDAL and II is for verify the the contribution of each constraint in the proposed CRD as well as the advantages of our design on the feature-level distillation. A visualization is also presented to show the benefits of CRD in improving the representation ability of EDGCN.

**Effectiveness of learning modules in EDAL** In the setup I, we split the EDAL into two parts. (i) AAG: Attentive feature aggregation based on the obtained joint representation of all attributes; (ii) UPD<sub>U</sub>: Updating function for refining coordinate attributes layer-by-layer. We can conclude from Eq. V that our approach can attain competitive performance on

TABLE V  
THE ABLATION STUDY ON THE EFFECTS OF DIFFERENT DESIGNS TO MODEL’S PERFORMANCE.

|    | EDGCN            |                  | $\mathcal{L}_{infer}$ | $\mathcal{L}_{feat}$ |   |   |   | N-Cal        | CIF10        |
|----|------------------|------------------|-----------------------|----------------------|---|---|---|--------------|--------------|
|    | AAG <sup>†</sup> | UPD <sub>U</sub> |                       | A                    | B | C | D |              |              |
| I  | ✓                |                  |                       |                      |   |   |   | 0.783        | 0.694        |
|    | ✓                | ✓                |                       |                      |   |   |   | 0.801        | 0.716        |
| II | ✓                | ✓                | ✓                     |                      |   |   |   | 0.818        | 0.724        |
|    | ✓                | ✓                | ✓                     | ✓                    |   |   |   | 0.825        | 0.733        |
|    | ✓                | ✓                | ✓                     |                      | ✓ |   |   | 0.830        | 0.749        |
|    | ✓                | ✓                | ✓                     |                      |   | ✓ |   | <b>0.835</b> | <b>0.752</b> |
|    | ✓                | ✓                | ✓                     |                      |   |   | ✓ | 0.814        | 0.721        |

<sup>†</sup>: AAG represents the architecture of EDAL without coordinate attribute updating module (UPD<sub>U</sub>).

recognition tasks even without UPD<sub>U</sub>, suggesting the effectiveness of our design on neighborhood definition. Also, we can see that UPD<sub>U</sub> further brings considerable improvement, indicating that the coordinate attribute strengthened by UPD<sub>U</sub> can further facilitate the aggregation process.

**Designs in the CRD** Variants A, B, and C represent three knowledge transfer designs in the intermediate feature-level mentioned in Eq. 4, respectively. The three variants all adopt the contrastive loss to encourage the consistency between teacher and student features. Their difference is that, compared to merely use the contrastive loss, B additionally appends task-specific loss to the intermediate layers in both the student and teacher branches while this task-specific loss is only inserted to the teacher in C. The difference between variant D and A is that it uses hard constraints such as the L1 loss [19] to alternate the contrastive loss utilized in A for feature distillation.

Eq. V shows that the inference-level distillation brings noticeable improvement than training EDGCN individually and variants A, B, and C can further improve the performance of EDGCN relying on the supervision provided by intermediate features, where B achieves the best result. We attribute this to the fact that the application of  $\mathcal{L}_{task}$  on the intermediate features of the frame-based model forces the teacher to represent the input events more comprehensively, thereby providing better intermediate guidance to the student. Interestingly, B performs weaker than C, even with additional task-specific loss for the student. We attribute the reason to that intermediate features in the graph model are not powerful enough for reliable prediction and such a inference-level loss in the intermediate level may be conflict with the feature contrastive loss for the student. Besides, we find that variant D damages the entire learning framework. We think that the considerable discrepancy between the two models causes their learned logic to be distinct. Therefore, variant dimensions of intermediate features from two networks might encode different semantics [53], making hard constraints unreasonable choices to achieve feature-level consistency. This observation supports our motivation of applying contrastive learning loss for the image-to-graph feature-level distillation.

**Visualization for feature representation** We further illus-

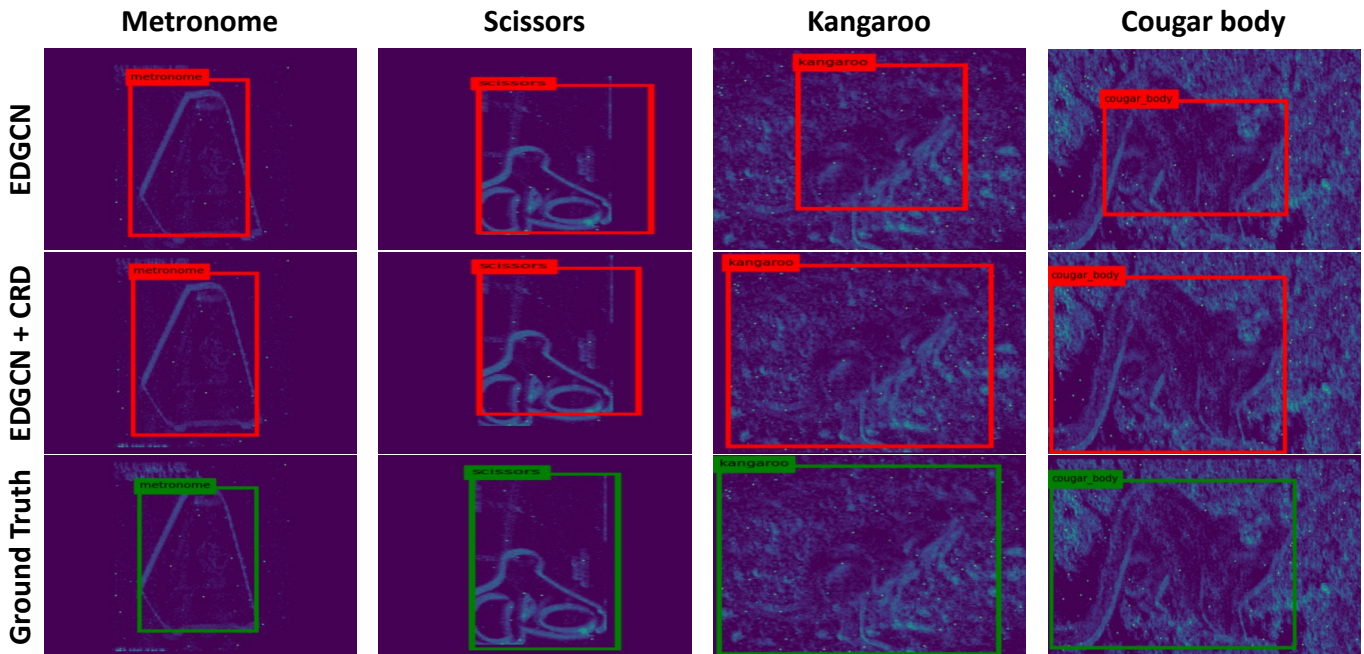


Fig. 5. Qualitative results of the detection task performed by the proposed EDGCN and CRD on N-Cal [54] dataset. Specifically, we show examples correctly categorized by the model and analyze their object localization ability. It can be seen that, although it is easy for EDGCN trained solely to recognize and localize the simple objects in the first two columns, there exists hardness to do the same thing on the event-based samples with complex background textures. In the last two columns, we show that after applying the CRD, we have mitigated to a certain extent the adverse effects on network localization caused by the interference of complex background textures, illustrating the promotion brought by the CRD on feature learning of the EDGCN. Best viewed in color.

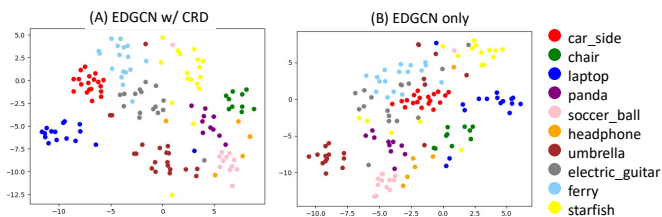


Fig. 6. The t-SNE visualization on the test set of N-Cal.

trate t-SNE of features on the N-Cal dataset in Eq. 6. The EDGCN trained solely shows weakness in achieving explicit decision boundaries among some challenging classes such as *car\_side* and *ferry* due to their similar appearances (Eq. 6.(B)). This limitation of EDGCN can be mitigated by CRD, where more discriminative features are obtained (Eq. 6.(A)), indicating the efficacy of CRD in boosting the representation ability of EDGCN.

## V. CONCLUSION

We present a novel dynamic graph CNN (EDGCN) for event-based learning. The EDGCN can define the neighborhood precisely for each event-based vertex considering all its attributes and dynamically update vertices’ attributes layer-by-layer. Besides, we introduce the cross-representation distillation scheme (CRD) for point-based methods, which exploits the large-scale prior from frame-based models to facilitate the training of the EDGCN. Comprehensive experiments on various vision tasks validate the efficacy of our EDGCN and

CRD. Moreover, since the CRD holds potential in migrating to other point-based methods for event data, we argue that this learning strategy may open a new research path on the learning of event-based models.

## APPENDIX A NETWORK STRUCTURE

TABLE VI  
SETTINGS OF NETWORK STRUCTURES.

|           | Layer 1 | Layer 2 | Layer 3 |
|-----------|---------|---------|---------|
| $in D_u$  | 3       | 25      | 64      |
| $in D_f$  | 25      | 64      | 64      |
| $out D_f$ | 64      | 64      | 128     |
| $N_n$     | 20      | 20      | 20      |

As stated in the main manuscript, we keep the network structure of the proposed EDGCN unchanged for all datasets except for its task head. Here, we detail the structure settings of three feature aggregation layers (EDALs) in our model (Eq. VI).

## APPENDIX B ROBUSTNESS TO THE TIME SPAN OF INPUT EVENTS

We follow the experiment settings adopted in [3], [31] to validate the robustness of our approach to the time span of input events. For instance, if a learning model takes event signals with 100ms length as input, the time span of input events should be 100ms. We compare our model with two



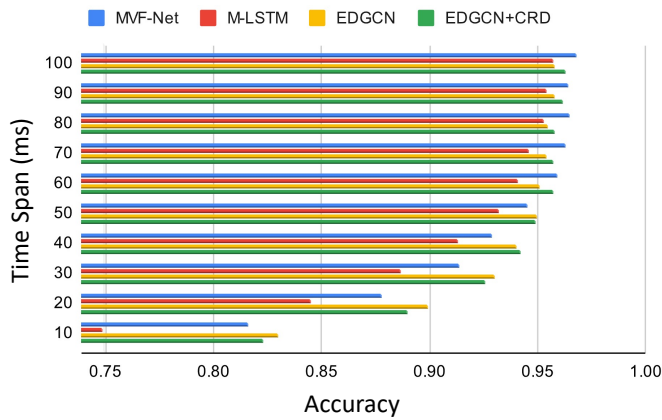


Fig. 7. Analysis of event-based methods *w.r.t* the time span of input events and classification accuracy. Best viewed in color.

SOTA frame-based approaches (MVF-Net [5], and M-LSTM [3]) on a series of testing settings using the N-C dataset and present results in Fig. 7. The testing set contains event samples with variable time duration (10% ~ 100%). We can see that though the best performance of our model is slightly lower than frame-based approaches, the robustness of our model to the time span of input events is better than their methods, especially with the short time span input, showing the reliability of our method in processing event data under complex working conditions.

## APPENDIX C

### COMPARE TO MOST RELATIVE STUDIES.

The most relative works to our approach are VGCNN [14] and VMV-GCN [15] since their studies adopt the same type of input representations as our approach. However, unlike their works with biased feature aggregation (e.g., merely considering spatiotemporal distances in [15]) or handcrafted scaling weights (e.g., [14]), we remove this bottleneck by considering all attributes in a learnable manner. In specific, [14] uses original input coordinates to find and aggregate neighboring vertices while original coordinates may not be able to distinguish the proximity of vertices in the feature space. To solve the shortcoming of [14], [15] defines neighborhood space by updating coordinate attributes. Yet, [15] only relies on the geometric relationship between vertices and ignores the semantic relationship. The major novelty of EDGCN is how to define neighborhood space for each vertex by considering all attributes based on semantics & spatial-temporal features adaptively. Besides, the proposed EDGCN introduces attentive feature aggregation for neighbor feature embedding, which is more flexible than [15] which just uses a Max pooling for hard aggregating. In addition, we propose a novel distillation scheme for point-based approaches which is capable of improving the performance of our approach step further.

## REFERENCES

[1] G. Gallego, T. Delbruck, G. M. Orchard, C. Bartolozzi, B. Taba, A. Censi, S. Leutenegger, A. Davison, J. Conradt, K. Daniilidis, and

D. Scaramuzza, “Event-based vision: A survey,” *IEEE Trans. Pattern Anal. Mach. Intell.*, pp. 1–1, 2020.

[2] D. Gehrig, A. Loquercio, K. G. Derpanis, and D. Scaramuzza, “End-to-end learning of representations for asynchronous event-based data,” in *IEEE/CVF Int. Conf. Comput. Vis.*, 2019, pp. 5633–5643.

[3] M. Cannici, M. Ciccone, A. Romanoni, and M. Matteucci, “A differentiable recurrent surface for asynchronous event-based data,” in *Eur. Conf. Comput. Vis.*, August 2020.

[4] N. Messikommer, D. Gehrig, A. Loquercio, and D. Scaramuzza, “Event-based asynchronous sparse convolutional networks,” in *Eur. Conf. Comput. Vis.* Springer, 2020, pp. 415–431.

[5] Y. Deng, H. Chen, and Y. Li, “Mvf-net: A multi-view fusion network for event-based object classification,” *IEEE Trans. Circuits Syst. Video Technol.*, pp. 1–1, 2021.

[6] R. Baldwin, R. Liu, M. M. Almatrafi, V. K. Asari, and K. Hirakawa, “Time-ordered recent event (tore) volumes for event cameras,” *IEEE Trans. Pattern Anal. Mach. Intell.*, pp. 1–1, 2022.

[7] H. Rebecq, R. Ranftl, V. Koltun, and D. Scaramuzza, “High speed and high dynamic range video with an event camera,” *IEEE Trans. Pattern Anal. Mach. Intell.*, pp. 1–1, 2019.

[8] C. R. Qi, H. Su, K. Mo, and L. J. Guibas, “Pointnet: Deep learning on point sets for 3d classification and segmentation,” in *IEEE Conf. Comput. Vis. Pattern Recog.*, 2017, pp. 652–660.

[9] Q. Wang, Y. Zhang, J. Yuan, and Y. Lu, “Space-time event clouds for gesture recognition: From rgb cameras to event cameras,” in *IEEE Winter Conf. on Appl. of Comput. Vis.*, 2019, pp. 1826–1835.

[10] Y. Sekikawa, K. Hara, and H. Saito, “Eventnet: Asynchronous recursive event processing,” in *IEEE Conf. Comput. Vis. Pattern Recog.*, June 2019.

[11] Y. Bi, A. Chadha, A. Abbas, E. Bourtsoulatze, and Y. Andreopoulos, “Graph-based spatio-temporal feature learning for neuromorphic vision sensing,” *IEEE Trans. Image Process.*, pp. 1–1, 2020.

[12] Y. Li, H. Zhou, B. Yang, Y. Zhang, Z. Cui, H. Bao, and G. Zhang, “Graph-based asynchronous event processing for rapid object recognition,” in *IEEE/CVF Int. Conf. Comput. Vis.*, 2021, pp. 914–923.

[13] S. Schaefer, D. Gehrig, and D. Scaramuzza, “Aegnn: Asynchronous event-based graph neural networks,” in *IEEE Conf. Comput. Vis. Pattern Recog.*, 2022.

[14] Y. Deng, H. Chen, H. Liu, and Y. Li, “A voxel graph cnn for object classification with event cameras,” in *IEEE Conf. Comput. Vis. Pattern Recog.*, June 2022, pp. 1172–1181.

[15] B. Xie, Y. Deng, Z. Shao, H. Liu, and Y. Li, “Vmv-gcn: Volumetric multi-view based graph cnn for event stream classification,” *IEEE Robot. Autom. Lett.*, vol. 7, no. 2, pp. 1976–1983, 2022.

[16] Z. Li, M. S. Asif, and Z. Ma, “Event transformer,” *arXiv preprint arXiv:2204.05172*, 2022.

[17] T. Chen, S. Kornblith, M. Norouzi, and G. Hinton, “A simple framework for contrastive learning of visual representations,” in *Int. Conf. Mach. Learn.* PMLR, 2020, pp. 1597–1607.

[18] G. Hinton, O. Vinyals, and J. Dean, “Distilling the knowledge in a neural network,” in *NIPS Deep Learning and Representation Learning Workshop*, 2015.

[19] A. Romero, N. Ballas, S. E. Kahou, A. Chassang, C. Gatta, and Y. Bengio, “Fitnets: Hints for thin deep nets,” in *Int. Conf. Learn. Represent.*, 2015.

[20] A. Zanardi, A. Aumiller, J. Zilly, A. Censi, and E. Frazzoli, “Cross-modal learning filters for rgb-neuromorphic wormhole learning,” *Robotics: Science and System XV*, p. P45, 2019.

[21] Y. Hu, T. Delbruck, and S.-C. Liu, “Learning to exploit multiple vision modalities by using grafted networks,” in *Eur. Conf. Comput. Vis.*, 2020, pp. 85–101.

[22] Y. Deng, H. Chen, H. Chen, and Y. Li, “Learning from images: A distillation learning framework for event cameras,” *IEEE Trans. Image Process.*, pp. 1–1, 2021.

[23] Z. Sun, N. Messikommer, D. Gehrig, and D. Scaramuzza, “Ess: Learning event-based semantic segmentation from still images,” in *Eur. Conf. Comput. Vis.* Springer, 2022, pp. 341–357.

[24] X. Zhang, W. Liao, L. Yu, W. Yang, and G.-S. Xia, “Event-based synthetic aperture imaging with a hybrid network,” in *IEEE Conf. Comput. Vis. Pattern Recog.*, 2021, pp. 14 235–14 244.

[25] L. Zhu, X. Wang, Y. Chang, J. Li, T. Huang, and Y. Tian, “Event-based video reconstruction via potential-assisted spiking neural network,” in *IEEE Conf. Comput. Vis. Pattern Recog.*, June 2022, pp. 3594–3604.

[26] A. Zihao Zhu, L. Yuan, K. Chaney, and K. Daniilidis, “Unsupervised event-based optical flow using motion compensation,” in *Eur. Conf. Comput. Vis.*, 2018, pp. 0–0.

- [27] J. Hagenaars, F. Paredes-Vallés, and G. De Croon, “Self-supervised learning of event-based optical flow with spiking neural networks,” *Advances in Neural Information Processing Systems*, vol. 34, pp. 7167–7179, 2021.
- [28] L. Hu, R. Zhao, Z. Ding, L. Ma, B. Shi, R. Xiong, and T. Huang, “Optical flow estimation for spiking camera,” in *IEEE Conf. Comput. Vis. Pattern Recog.*, June 2022, pp. 17 844–17 853.
- [29] A. Mitrokhin, Z. Hua, C. Fermuller, and Y. Aloimonos, “Learning visual motion segmentation using event surfaces,” in *IEEE Conf. Comput. Vis. Pattern Recog.*, 2020, pp. 14 414–14 423.
- [30] G. Orchard, C. Meyer, R. Etienne-Cummings, C. Posch, N. Thakor, and R. Benosman, “Hfirst: A temporal approach to object recognition,” *IEEE Trans. Pattern Anal. Mach. Intell.*, vol. 37, no. 10, pp. 2028–2040, Oct 2015.
- [31] A. Sironi, M. Brambilla, N. Bourdis, X. Lagorce, and R. Benosman, “Hats: Histograms of averaged time surfaces for robust event-based object classification,” in *IEEE Conf. Comput. Vis. Pattern Recog.*, 2018, pp. 1731–1740.
- [32] Z. Wu, H. Zhang, Y. Lin, G. Li, M. Wang, and Y. Tang, “Liaf-net: Leaky integrate and analog fire network for lightweight and efficient spatiotemporal information processing,” *IEEE Transactions on Neural Networks and Learning Systems*, vol. 33, no. 11, pp. 6249–6262, 2022.
- [33] M. Yao, H. Gao, G. Zhao, D. Wang, Y. Lin, Z. Yang, and G. Li, “Temporal-wise attention spiking neural networks for event streams classification,” in *Int. Conf. Comput. Vis.*, 2021, pp. 10 221–10 230.
- [34] H. Rebecq, R. Ranftl, V. Koltun, and D. Scaramuzza, “High speed and high dynamic range video with an event camera,” *IEEE Trans. Pattern Anal. Mach. Intell.*, pp. 1–1, 2019.
- [35] L. Wang, T.-K. Kim, and K.-J. Yoon, “Eventsr: From asynchronous events to image reconstruction, restoration, and super-resolution via end-to-end adversarial learning,” in *IEEE Conf. Comput. Vis. Pattern Recog.*, 2020, pp. 8315–8325.
- [36] S. Tulyakov, A. Bochicchio, D. Gehrig, S. Georgoulis, Y. Li, and D. Scaramuzza, “Time lens++: Event-based frame interpolation with parametric non-linear flow and multi-scale fusion,” in *IEEE Conf. Comput. Vis. Pattern Recog.*, 2022, pp. 17 755–17 764.
- [37] L. Wang, Y. Chae, S.-H. Yoon, T.-K. Kim, and K.-J. Yoon, “Evdistill: Asynchronous events to end-task learning via bidirectional reconstruction-guided cross-modal knowledge distillation,” in *IEEE Conf. Comput. Vis. Pattern Recog.*, 2021, pp. 608–619.
- [38] N. Messikommer, D. Gehrig, M. Gehrig, and D. Scaramuzza, “Bridging the gap between events and frames through unsupervised domain adaptation,” *IEEE Robot. Autom. Lett.*, vol. 7, no. 2, pp. 3515–3522, 2022.
- [39] D. Gehrig, M. Gehrig, J. Hidalgo-Carrió, and D. Scaramuzza, “Video to events: Recycling video datasets for event cameras,” in *IEEE Conf. Comput. Vis. Pattern Recog.*, June 2020.
- [40] T. Delbruck, Y. Hu, and Z. He, “V2E: From video frames to realistic DVS event camera streams,” *arxiv*, Jun. 2020. [Online]. Available: <http://arxiv.org/abs/2006.07722>
- [41] H. Rebecq, D. Gehrig, and D. Scaramuzza, “Esim: an open event camera simulator,” in *Conf. on Robot Learn.* PMLR, 2018, pp. 969–982.
- [42] C. R. Qi, L. Yi, H. Su, and L. J. Guibas, “Pointnet++: Deep hierarchical feature learning on point sets in a metric space,” in *Conf. Neural Inf. Process. Syst.*, 2017, pp. 5099–5108.
- [43] J. Redmon, S. Divvala, R. Girshick, and A. Farhadi, “You only look once: Unified, real-time object detection,” in *IEEE Conf. Comput. Vis. Pattern Recog.*, 2016, pp. 779–788.
- [44] P. Isola, J.-Y. Zhu, T. Zhou, and A. A. Efros, “Image-to-image translation with conditional adversarial networks,” in *IEEE Conf. Comput. Vis. Pattern Recog.*, 2017.
- [45] S. Huang, Y. Xie, S.-C. Zhu, and Y. Zhu, “Spatio-temporal self-supervised representation learning for 3d point clouds,” in *IEEE Conf. Comput. Vis. Pattern Recog.*, 2021, pp. 6535–6545.
- [46] G. Orchard, A. Jayawant, G. K. Cohen, and N. Thakor, “Converting static image datasets to spiking neuromorphic datasets using saccades,” *Front. Neurosci.*, vol. 9, p. 437, 2015.
- [47] H. Li, H. Liu, X. Ji, G. Li, and L. Shi, “Cifar10-dvs: An event-stream dataset for object classification,” *Front. Neurosci.*, vol. 11, p. 309, 2017.
- [48] A. Amir, B. Taba, D. Berg, T. Melano, J. McKinstry, C. Di Nolfo, T. Nayak, A. Andreopoulos, G. Garreau, M. Mendoza *et al.*, “A low power, fully event-based gesture recognition system,” in *IEEE Conf. Comput. Vis. Pattern Recog.*, 2017, pp. 7243–7252.
- [49] K. He, X. Zhang, S. Ren, and J. Sun, “Deep residual learning for image recognition,” in *IEEE Conf. Comput. Vis. Pattern Recog.*, 2016, pp. 770–778.
- [50] C.-F. R. Chen, R. Panda, K. Ramakrishnan, R. Feris, J. Cohn, A. Oliva, and Q. Fan, “Deep analysis of cnn-based spatio-temporal representations for action recognition,” in *Proceedings of the IEEE/CVF Conference on Computer Vision and Pattern Recognition*, 2021, pp. 6165–6175.
- [51] J. Deng, W. Dong, R. Socher, L.-J. Li, K. Li, and L. Fei-Fei, “Imagenet: A large-scale hierarchical image database,” in *IEEE Conf. Comput. Vis. Pattern Recog.*, 2009, pp. 248–255.
- [52] M. Cannici, M. Ciccone, A. Romanoni, and M. Matteucci, “Asynchronous convolutional networks for object detection in neuromorphic cameras,” in *IEEE Conf. Comput. Vis. Pattern Recog. Workshops*, 2019, pp. 0–0.
- [53] M. A. Islam, M. Kowal, S. Jia, K. G. Derpanis, and N. D. B. Bruce, “Global pooling, more than meets the eye: Position information is encoded channel-wise in cnns,” in *Int. Conf. Comput. Vis.*, October 2021, pp. 793–801.
- [54] G. Orchard and R. Etienne-Cummings, “Bioinspired visual motion estimation,” *Proceedings of the IEEE*, vol. 102, no. 10, pp. 1520–1536, 2014.